

## ALFALFA DISCOVERY OF THE NEARBY GAS-RICH DWARF GALAXY LEO P. II. OPTICAL IMAGING OBSERVATIONS

KATHERINE L. RHODE<sup>1</sup>, JOHN J. SALZER<sup>1,2</sup>, NATHALIE C. HAURBERG<sup>1</sup>, ANGELA VAN SISTINE<sup>1,2</sup>, MICHAEL D. YOUNG<sup>1</sup>,  
 MARTHA P. HAYNES<sup>3</sup>, RICCARDO GIOVANELLI<sup>3</sup>, JOHN M. CANNON<sup>4</sup>, EVAN D. SKILLMAN<sup>5</sup>, KRISTEN B. W. MCQUINN<sup>5</sup>, &  
 ELIZABETH A. K. ADAMS<sup>3</sup>

*Accepted to AJ on 2 April 2013*

### ABSTRACT

We present results from ground-based optical imaging of a low-mass dwarf galaxy discovered by the ALFALFA 21-cm H I survey. Broadband (BVR) data obtained with the WIYN 3.5-m telescope at Kitt Peak National Observatory (KPNO) are used to construct color-magnitude diagrams of the galaxy's stellar population down to  $V_o \sim 25$ . We also use narrowband H $\alpha$  imaging from the KPNO 2.1-m telescope to identify an H II region in the galaxy. We use these data to constrain the distance to the galaxy to be between 1.5 and 2.0 Mpc. This places Leo P within the Local Volume but beyond the Local Group. Its properties are extreme: it is the lowest-mass system known that contains significant amounts of gas and is currently forming stars.

*Subject headings:* galaxies: irregular — galaxies: dwarf — galaxies: distances and redshifts — galaxies: photometry — galaxies: stellar content

### 1. INTRODUCTION

The number of known galaxies in and around the Local Group (LG) is increasing with time, as new dwarf galaxies are discovered serendipitously in wide-field surveys and via dedicated searches (e.g., Armandroff, Davies, & Jacoby 1998, Karachentsev et al. 2000, Willman et al. 2005, Whiting et al. 2007). The 1998 review article by Mateo on dwarf galaxies in the LG lists  $\sim 38$  dwarfs in its census. A recent review by McConnachie (2012) summarized the observed properties of nearby dwarf galaxies and listed  $\sim 70$  “definite” or “very likely” LG dwarfs and a total of more than 90 dwarf galaxies within 3 Mpc of the Sun. McConnachie notes that not only has the number of nearby dwarf galaxies essentially doubled over roughly the last decade, but improvements in observing capabilities over the same time period have enabled us to study the star formation histories and other properties of dwarf galaxies in much more detail (e.g., Tolstoy et al. 2009 and references therein). The newly-identified low-mass systems give us a more complete census of the Local Volume and provide a testing ground for ideas and theories that are fundamental to many areas of astrophysics — ideas about chemical evolution, star formation, stellar feedback processes, galaxy evolution, hierarchical galaxy assembly, and dark matter (e.g., Tolstoy et al. 2009).

The majority of recently discovered dwarf galaxies lo-

cated within the LG or in the immediate vicinity are gas-poor dwarf spheroidal (dSph) galaxies and/or ultra-low-luminosity systems that have been detected as small surface brightness enhancements or slight overdensities of stars (e.g., Martin et al. 2006, Belokurov et al. 2007, Bell, Slater, & Martin 2011). Only a few have detectable amounts of gas (e.g., Phoenix: Canterna & Flower 1977, Young et al. 2007; Leo T: Irwin et al. 2007), and these tend to be located relatively far from the two giant members of the LG, Andromeda and the Milky Way. In contrast to the small number of dwarfs with gas, wide area 21-cm radio surveys have cataloged hundreds of H I clouds with velocities that potentially place them in and around the LG (Blitz et al. 1999; Braun & Burton 1999; Giovanelli et al. 2010). In the current paper, we present optical observations of one such object, the gas-rich galaxy AGC 208583 (= Leo P), discovered by the ALFALFA H I survey (Giovanelli et al. 2005; Haynes et al. 2011) and described in Giovanelli et al. (2013).

We have obtained ground-based narrowband H $\alpha$  and broadband BVR images of Leo P and made photometric measurements of the resolved stellar population detected in the data. We use these optical data to construct color-magnitude diagrams (CMDs) of the galaxy's stellar component. These CMDs are used to constrain the distance to the galaxy and show that Leo P is likely to be located between 1.5 and 2.0 Mpc from the Milky Way. In addition, we highlight the unusual nature of this system by quantifying its physical properties (e.g., size, H $\alpha$  luminosity, V-band luminosity, colors, and H I stellar mass).

### 2. OBSERVATIONS

#### 2.1. Broadband BVR Imaging

The WIYN Observatory<sup>6</sup> 3.5-m telescope was used on 26 March 2012 to image the field located at the position of an ALFALFA detection at 10h 21m 45.0s +18d

<sup>6</sup> The WIYN Observatory is a joint facility of the University of Wisconsin-Madison, Indiana University, Yale University, and the National Optical Astronomy Observatory.

<sup>1</sup> Department of Astronomy, Indiana University, 727 East Third Street, Bloomington, IN 47405. *e-mail:* rhode@astro.indiana.edu, slaz@astro.indiana.edu

<sup>2</sup> Visiting Astronomer, Kitt Peak National Observatory, National Optical Astronomy Observatory, which is operated by the Association of Universities for Research in Astronomy (AURA) under cooperative agreement with the National Science Foundation.

<sup>3</sup> Center for Radiophysics and Space Research, Space Sciences Building, Cornell University, Ithaca, NY 14853. *e-mail:* riccardo@astro.cornell.edu, haynes@astro.cornell.edu, betsey@astro.cornell.edu

<sup>4</sup> Department of Physics and Astronomy, Macalester College, Saint Paul, MN 55105. *e-mail:* jcannon@macalester.edu

<sup>5</sup> Minnesota Institute for Astrophysics, University of Minnesota, Minneapolis, MN 55455. *e-mail:* skillman@astro.umn.edu, mcquinn@astro.umn.edu

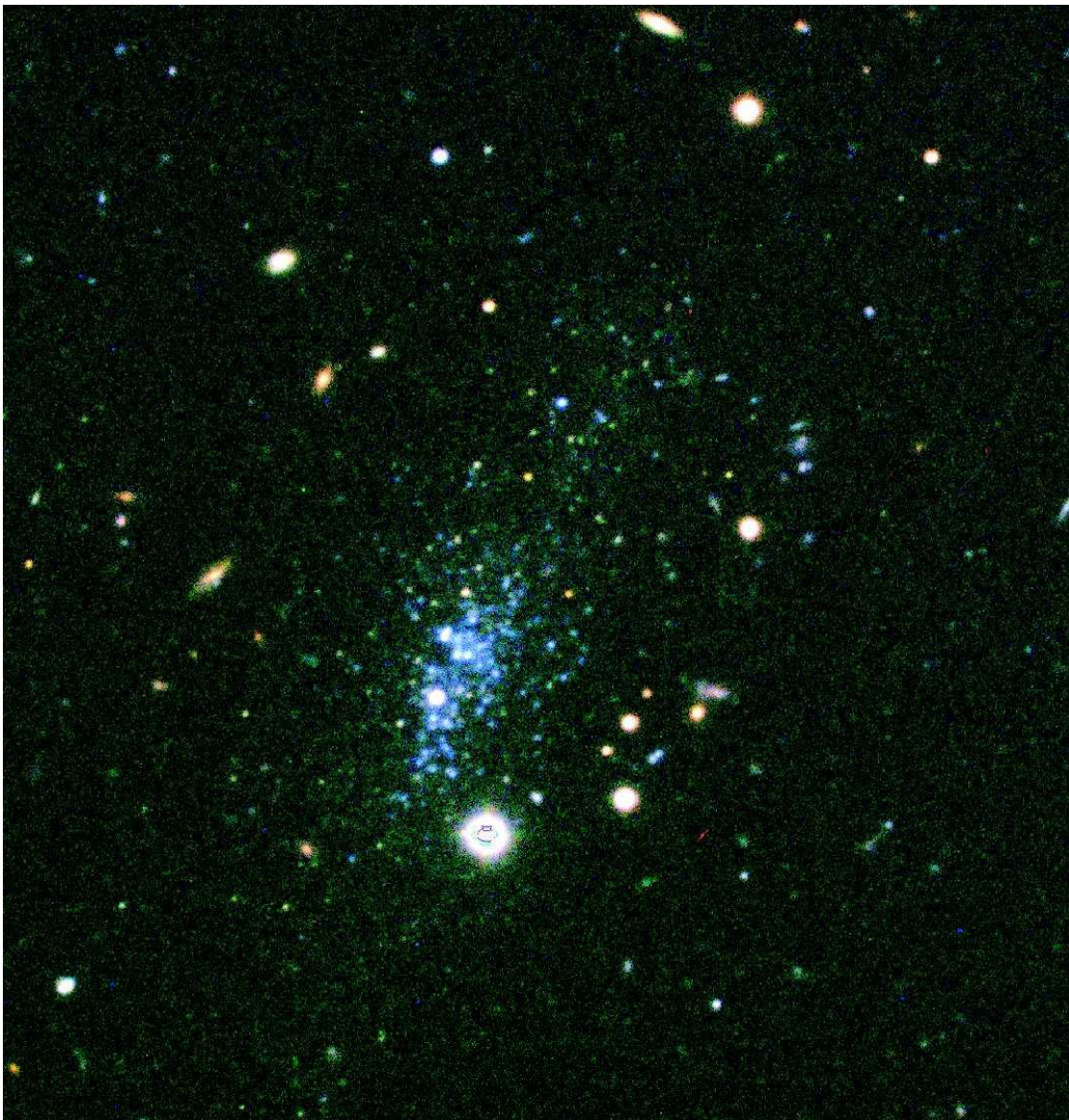


FIG. 1.— BVR color composite image of Leo P obtained with the WIYN 3.5-m telescope. The FOV of this image is  $2.4'$  by  $2.5'$  and the orientation is N-up, E-left. The lower (southern) portion of Leo P is dominated by a clump of blue stars, indicating very recent star formation has occurred. The brightest object in Leo P (located above and to the left of the bright foreground star) is an HII region that appears to be photoionized by an O or B-type star or stellar association. The upper portion of the galaxy is very low surface brightness but includes a number of redder stars, presumably RGB members in Leo P. The total size of the galaxy at this sensitivity level is  $\sim 90''$ .

05m 01s. These observations revealed an optical counterpart with a resolved stellar component. All observations were obtained with the Minimosaic camera through standard BVR broadband filters under photometric conditions. Total integration times of 30 minutes in B, 24 minutes in V, and 20 minutes in R were achieved, split between two images for each filter. Stellar point-spread function (PSF) measurements ranged between  $0.6''$  and  $0.8''$  for the sequence of observations. Images of Landolt (1992) standard stars taken before and after the observations of Leo P provided photometric calibrations. Errors on the photometric coefficients were  $<0.01$  mag. Data reduction followed normal practices.

A composite three-color image of Leo P is shown in Figure 1. The image is oriented N-up E-left. The galaxy is resolved into stars, with a strong concentration of the

brightest and bluest stars appearing in the southern portion. As we discuss in §3, these may be upper main-sequence stars with B and A spectral types. A number of fainter and redder stars are also present that are presumably red giants from an older population. These redder stars appear to be uniformly distributed throughout the galaxy, although in the northern, lower-surface-brightness region they are the only stars present.

The angular diameter of the optical portion of the galaxy is  $\sim 90$  arcsec. The size of the galaxy could not easily be constrained via surface brightness measurements, so the diameter is based on the apparent extent of the stellar point sources. To measure the extent, we used the list of all point sources in the image with color errors less than 0.25 mag (see Section 3). We assigned each of the point sources to one of a series of 0.05-arcmin-wide



concentric annuli centered on the approximate midpoint of the galaxy light distribution. An effective area was calculated for each annulus that excluded portions of the annulus that extended off the edge of the image. The number of point sources in each annulus was then divided by the effective area of the annulus to produce a radial profile (surface density of stars versus projected radius) of the stellar distribution. The surface density falls to the level of the background stellar density at  $0.725$  arcmin from the galaxy center; from this we estimate that the apparent diameter of the galaxy is  $87$  arcsec with an uncertainty of  $\pm 3$  arcsec (the width of one annulus). The photometric properties of the stars in Leo P are discussed in detail in the next section.

## 2.2. $H\alpha$ Imaging

Narrowband  $H\alpha$  images of Leo P were obtained with the KPNO 2.1-m telescope on 20 March 2012. The observations consist of two 15-minute exposures taken with a narrowband filter (central  $\lambda = 6573$  Å, bandwidth =  $67$  Å) sandwiched around a single 3-minute R-band image that was used for continuum subtraction. An additional 15-minute R-band image was taken to provide a deeper exposure of the system. Standard image processing steps were utilized to produce a continuum-subtracted image of Leo P in the light of the  $H\alpha$  emission line (Figure 2). Observations of spectrophotometric standard stars (Oke & Gunn 1983) allowed us to calibrate the observed narrowband flux.

Figure 2 shows that Leo P possesses a single H II region located near the southern end of the galaxy. The H II region is associated with a bright, blue star and appears as the single brightest object in the system. The H II region is spatially resolved, and has an apparent diameter of  $1.20 \pm 0.05$  arcsec. The observed emission-line flux is  $(1.71 \pm 0.03) \times 10^{-14}$  erg/s/cm<sup>2</sup>. Our narrow-band data are quite sensitive, with a  $5\sigma$  point source detection limit of  $\sim 5.0 \times 10^{-17}$  erg/s/cm<sup>2</sup>.

## 3. PHOTOMETRY AND CMDS OF LEO P

We utilized the PSF-fitting photometry software DAOPHOT (Stetson 1987, 1990) to measure the brightnesses of the stars in the broadband BVR images obtained with the WIYN 3.5-m telescope. A model PSF was constructed using a selection of foreground stars as well as relatively bright, isolated stars believed to be members of Leo P. Photometry was performed on each broadband image using a list of stars selected from a combined R and V image and allowing the program to redetermine the precise position of the centroids in each frame independently. We calculated and applied aperture corrections to the results and calibrated the apparent magnitudes using the photometric solution derived from the Landolt standard star observations. As a check of the PSF-fitting photometry, we measured the fluxes from isolated single stars using aperture photometry methods. These checks verified the integrity of the DAOPHOT results.

Color-magnitude diagrams (CMDs) of the resolved stars in Leo P are shown in Figure 3. We present CMDs in two colors:  $(B-V)_o$  (Figure 3a) and  $(V-R)_o$  (Figure 3b). All stars brighter than  $V_o \sim 25.0$  have been measured, but only stars with color errors less than  $0.25$  mag are included in the plots ( $N=82$  for the  $(B-V)_o$  plot

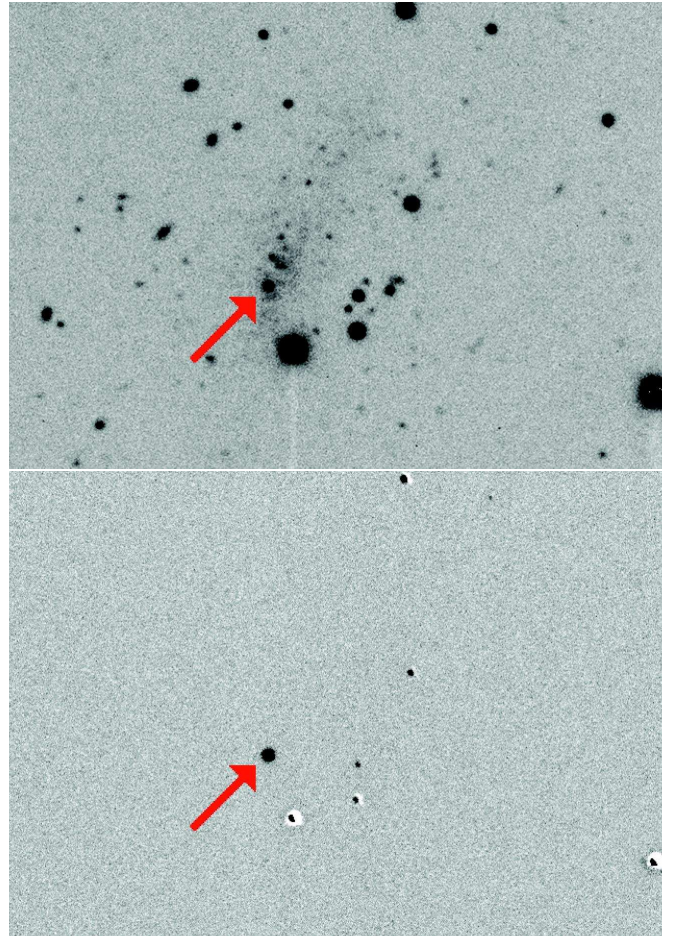


FIG. 2.— Narrowband imaging of Leo P. The left panel is an R-band continuum image and the right panel is a continuum-subtracted  $H\alpha$  image, both taken with the KPNO 2.1m telescope. The images are oriented N-up, E-left. There is a single HII region present in Leo P (location marked with an arrow in both panels), with an integrated flux of  $1.7 \times 10^{-14}$  erg/s/cm<sup>2</sup>. The points of emission to the right of the HII region in the right-hand panel are caused by imperfect continuum subtraction in some of the brighter stars.

and  $N=77$  for  $(V-R)_o$ ). The positions and photometric measurements of the 82 stars included in Figure 3a are listed in Table 1. All photometric quantities reported in this paper are corrected for Galactic absorption using  $E(B-V) = 0.026$  from Schlegel et al. (1998).

Unfortunately, our B photometry is relatively shallow, so the photometric uncertainties for the redder stars in Figure 3a are large. Likewise the R data are not as deep as the V data, leading to larger errors for the bluer stars in Figure 3b. Because of the differing depths of the images taken through the B, V and R filters, the main sequence (MS) in Leo P is better defined in the B–V plot, while the red giant branch has better definition in the V–R CMD. We performed a series of artificial star tests in order to quantify the point-source detection limits of the WIYN images. Thirty artificial stars with magnitudes within  $0.2$  mag of a fiducial value and the appropriate point spread function (PSF) were added to each of the combined images (B, V, and R). We then ran detection software to determine what fraction of these artificial objects would be recovered. We repeated this step in  $0.2$ -

magnitude intervals over a range of 4–5 magnitudes for each image. The result was a series of curves that quantify the completeness as a function of magnitude in each

of the combined images. Dashed lines in Figure 3 (and all subsequent CMD plots) show the 50% completeness levels of our data.

TABLE 1  
WIYN BROADBAND PHOTOMETRY OF RESOLVED STARS IN LEO P

#	RA (2000)	Dec (2000)	$V_o$	$\sigma_V$	$(B - V)_o$	$\sigma_{B-V}$	$(V - R)_o$	$\sigma_{V-R}$
1	10:21:45.1	+18:05:17.3	21.00	0.04	-0.19	0.04	0.12	0.05
2	10:21:45.0	+18:05:25.6	22.05	0.02	-0.14	0.03	0.00	0.03
3	10:21:44.9	+18:05:23.1	22.16	0.02	-0.19	0.03	-0.05	0.03
4	10:21:44.8	+18:05:23.0	22.36	0.02	-0.21	0.03	-0.08	0.04
5	10:21:43.9	+18:05:57.3	22.48	0.02	-0.12	0.03	-0.01	0.03
6	10:21:45.0	+18:05:26.3	22.53	0.02	-0.10	0.03	-0.03	0.04
7	10:21:44.8	+18:05:31.6	22.66	0.02	1.29	0.07	0.74	0.03
8	10:21:45.1	+18:05:14.5	22.98	0.04	-0.32	0.04	-0.05	0.06
9	10:21:44.8	+18:05:27.8	23.22	0.04	-0.18	0.05	0.11	0.06
10	10:21:45.0	+18:05:14.0	23.27	0.05	-0.24	0.06	0.18	0.08
11	10:21:45.5	+18:05:13.7	23.33	0.04	0.95	0.09	0.54	0.05
12	10:21:44.7	+18:05:48.8	23.34	0.04	0.96	0.08	0.65	0.05
13	10:21:44.7	+18:05:24.3	23.43	0.06	-0.32	0.07	-0.03	0.10
14	10:21:45.2	+18:05:21.0	23.43	0.04	-0.11	0.06	-0.07	0.08
15	10:21:44.0	+18:05:24.5	23.44	0.05	0.26	0.07	0.06	0.08
16	10:21:44.7	+18:05:34.9	23.50	0.04	0.91	0.10	0.59	0.06
17	10:21:44.6	+18:05:20.6	23.56	0.04	-0.08	0.06	0.11	0.08
18	10:21:45.0	+18:05:06.9	23.57	0.04	-0.12	0.07	-0.01	0.09
19	10:21:43.4	+18:05:38.8	23.58	0.05	0.72	0.10	0.58	0.07
20	10:21:44.9	+18:05:38.7	23.67	0.04	1.11	0.14	0.72	0.06
21	10:21:44.5	+18:05:32.6	23.69	0.08	0.01	0.10	...	...
22	10:21:44.7	+18:05:21.8	23.71	0.05	-0.35	0.07	-0.15	0.11
23	10:21:45.2	+18:05:09.8	23.75	0.06	-0.16	0.08	0.40	0.09
24	10:21:43.9	+18:05:52.3	23.76	0.06	1.21	0.18	0.65	0.08
25	10:21:45.2	+18:05:07.6	23.77	0.05	0.16	0.10	...	...
26	10:21:43.6	+18:05:41.7	23.78	0.06	0.79	0.13	0.55	0.09
27	10:21:44.2	+18:05:58.6	23.85	0.07	1.22	0.15	0.67	0.08
28	10:21:45.2	+18:05:13.3	23.87	0.07	-0.11	0.09	0.41	0.11
29	10:21:44.2	+18:05:53.2	23.87	0.07	0.95	0.16	0.62	0.08
30	10:21:45.1	+18:05:30.1	23.88	0.07	1.47	0.20	0.63	0.09
31	10:21:45.7	+18:04:57.2	23.89	0.05	1.01	0.17	0.49	0.08
32	10:21:45.0	+18:05:10.5	23.90	0.08	-0.22	0.10	0.13	0.11
33	10:21:45.3	+18:05:22.4	23.91	0.06	1.12	0.22	0.58	0.09
34	10:21:44.7	+18:05:16.9	23.95	0.06	-0.10	0.10	0.04	0.13
35	10:21:43.1	+18:06:02.6	23.96	0.07	1.02	0.17	0.73	0.09
36	10:21:44.5	+18:05:26.4	23.97	0.07	0.03	0.09	-0.10	0.14
37	10:21:43.6	+18:05:55.2	23.97	0.10	0.43	0.14	0.35	0.13
38	10:21:43.0	+18:05:59.8	24.00	0.08	0.38	0.11	0.57	0.11
39	10:21:45.0	+18:05:16.1	24.01	0.07	-0.32	0.09	-0.15	0.14
40	10:21:43.8	+18:05:26.1	24.04	0.09	0.12	0.12	0.09	0.14
41	10:21:44.4	+18:05:34.1	24.06	0.08	1.26	0.18	0.61	0.11
42	10:21:45.3	+18:05:06.4	24.06	0.07	0.72	0.15	0.59	0.09
43	10:21:44.0	+18:05:19.0	24.07	0.08	0.57	0.14	0.33	0.12
44	10:21:45.3	+18:05:08.5	24.07	0.07	-0.16	0.09	0.04	0.13
45	10:21:45.4	+18:05:03.6	24.09	0.06	0.02	0.09	0.18	0.11
46	10:21:45.2	+18:05:37.6	24.11	0.08	0.73	0.16	0.45	0.11
47	10:21:44.4	+18:05:30.1	24.13	0.08	0.19	0.12	0.27	0.11
48	10:21:43.8	+18:05:52.2	24.13	0.08	1.15	0.21	0.49	0.11
49	10:21:44.6	+18:05:22.2	24.16	0.08	-0.09	0.11	0.14	0.14
50	10:21:46.2	+18:05:05.8	24.16	0.08	1.06	0.18	0.47	0.12
51	10:21:44.0	+18:06:01.8	24.19	0.07	1.32	0.22	0.41	0.12
52	10:21:44.4	+18:05:26.0	24.23	0.10	0.03	0.14	-0.26	0.20
53	10:21:45.7	+18:05:25.8	24.23	0.08	0.94	0.20	...	...
54	10:21:45.3	+18:05:30.5	24.25	0.09	0.09	0.12	0.14	0.13
55	10:21:43.3	+18:06:01.3	24.25	0.11	1.13	0.22	0.75	0.13
56	10:21:44.7	+18:05:15.5	24.26	0.09	-0.17	0.11	...	...
57	10:21:44.8	+18:05:46.2	24.26	0.08	0.01	0.12	0.16	0.13
58	10:21:45.4	+18:05:31.9	24.27	0.09	0.68	0.17	0.92	0.11
59	10:21:44.0	+18:05:54.7	24.30	0.10	0.76	0.17	...	...
60	10:21:45.1	+18:05:11.7	24.30	0.09	0.06	0.14	-0.28	0.19
61	10:21:44.3	+18:05:18.1	24.33	0.10	0.07	0.14	...	...
62	10:21:43.0	+18:05:50.2	24.33	0.10	0.52	0.18	...	...
63	10:21:44.4	+18:05:27.5	24.36	0.10	0.89	0.23	0.48	0.14
64	10:21:44.6	+18:05:13.7	24.38	0.09	0.16	0.14	-0.05	0.18
65	10:21:44.4	+18:05:37.6	24.39	0.09	0.34	0.15	...	...
66	10:21:45.9	+18:05:21.3	24.39	0.07	0.03	0.12	0.16	0.15
67	10:21:45.9	+18:04:55.3	24.39	0.10	-0.15	0.12	-0.04	0.19
68	10:21:44.6	+18:05:29.3	24.42	0.10	0.14	0.15	-0.85	0.37
69	10:21:45.0	+18:05:38.2	24.43	0.13	0.11	0.17	0.23	0.18
70	10:21:44.8	+18:05:09.4	24.44	0.11	0.78	0.22	...	...
71	10:21:43.4	+18:05:48.3	24.46	0.09	0.57	0.18	...	...

TABLE 1 — *Continued*

#	RA (2000)	Dec (2000)	$V_o$	$\sigma_V$	$(B - V)_o$	$\sigma_{B-V}$	$(V - R)_o$	$\sigma_{V-R}$
72	10:21:44.2	+18:05:16.4	24.50	0.11	-0.01	0.15	0.15	0.18
73	10:21:44.7	+18:05:46.2	24.54	0.13	0.60	0.22	0.07	0.21
74	10:21:44.1	+18:05:34.5	24.55	0.10	0.43	0.20	...	...
75	10:21:44.9	+18:05:34.4	24.59	0.09	0.46	0.21	0.27	0.16
76	10:21:44.1	+18:05:40.5	24.60	0.12	0.29	0.15	...	...
77	10:21:44.0	+18:05:55.9	24.69	0.13	0.17	0.20	0.83	0.17
78	10:21:45.1	+18:05:39.0	24.72	0.12	-0.02	0.19	0.68	0.17
79	10:21:43.9	+18:05:46.9	24.73	0.12	0.52	0.22	...	...
80	10:21:43.7	+18:05:48.6	24.76	0.13	0.53	0.22	0.33	0.19
81	10:21:45.4	+18:05:36.5	24.81	0.13	0.39	0.23	...	...
82	10:21:45.0	+18:05:34.4	24.91	0.15	0.00	0.21	...	...

Two features are immediately apparent in the CMDs. First, a sequence of bright, blue stars is present in Leo P. The six brightest stars in our CMDs ( $V_o$  brighter than  $\sim 22.5$ ) all have  $(B - V)_o$  between  $-0.10$  and  $-0.21$ . The brightest object is the star located at the center of the single H II region (the first star in Table 1; hereafter Star 1). The photometry of this star has been corrected for nebular contamination using the emission-line spectrum obtained by our group and described below. Second, a red giant branch (RGB) appears to be present at  $(B - V)_o \sim 0.7 - 1.3$  and  $(V - R)_o \sim 0.4 - 0.8$ , beginning at  $V_o \sim 23.3$  and extending to fainter magnitudes. Unfortunately, the apparent location of the upper end of the RGB coincides with the onset of larger photometric errors in our data, making a secure identification of the RGB tip problematic. We return to this issue in §4.1.1 below.

Figure 4 presents the results of an analysis of the PSF photometry for the entire field of view included in our images of Leo P. The upper left plot (panel a) shows the data for the stars in Leo P; this is identical to Figure 3a. In the upper right plot (panel b) we show the corresponding CMD for the entire CCD frame, with the area covered by Leo P excluded. This plot shows the locations of the foreground stars and unresolved galaxies in the Leo P field (all obviously extended galaxies have been removed). When the two panels are compared, it is immediately obvious that the bright, blue stars in the Leo P area are completely absent from the full-field CMD. There are 13 stars in the Leo P area with  $(B - V)_o$  colors less than 0.0 and with  $V_o$  magnitudes brighter than 23.6, whereas there is not a single star in the rest of the image that falls within this range, despite the fact that the area covered in panel (b) is 51.3 times larger. Hence, there can be no question that the bright blue stars seen in Figure 1 are all associated with Leo P.

The lower two panels of Figure 4 show the CMDs for two random fields located in our CCD frames. The areas of the two regions are identical to that covered by Leo P (0.875 sq. arcmin). The fields are centered on the same declination as the Leo P area, but are offset by  $\sim 3$  arcmin in RA, one to the east and one to the west. These fields can be thought of as representing the foreground (or background) contamination present in the Leo P CMD. The two fields contain 6 and 9 stars, respectively, but only one star per field with  $V_o$  magnitudes brighter than 23.8. This suggests that foreground contamination of the Leo P CMD, especially at  $V_o$  brighter than  $\sim 24.0$ , is minimal. We quantify the contamination level of the Leo P CMD in the RGB region of the diagram

in §4.1.1.

In Figure 5 we replot the data shown in Figure 3a with model isochrones overlaid. The isochrones are from the Padova group (Girardi et al. 2002) for a 10 Myr old population with a metallicity ( $Z$ ) of 0.0004 (1/50th solar). The isochrones are plotted for four different distances: 0.5 Mpc (green), 1.0 Mpc (red), 1.5 Mpc (blue), and 2.0 Mpc (magenta). The values for age and  $Z$  were selected to be reasonable matches for Leo P (see §4.2), but in fact the locations of the isochrones change only slightly if different (but similar) ages or metallicities are used. To illustrate this last point, we plot a single 20 Myr isochrone for  $D = 1.5$  Mpc (dashed blue line).

We stress that these young-population isochrones cannot be used effectively to constrain the distance to Leo P, since the only portion of the CMD that is well defined is the upper MS, where the isochrones are nearly vertical. The only distinction between the Girardi et al. (2002) isochrones of different distances in the upper-MS region is a small color shift. By the time the MS starts to flatten slightly at colors redder than  $(B - V)_o = 0.0$ , the photometric errors for the MS stars are far too large to allow us to discriminate between the various isochrones.

It is worth noting that the five stars in Figure 5 with the smallest photometric errors ( $V_o$  between 22.0 and 22.6 with blue colors) are all located redward of the isochrones being displayed. This could be due to localized enhancement in the internal reddening in Leo P at their locations, or to the fact that these five stars are older than 10–20 Myr. This latter possibility would mean that they are likely to be post-MS stars: blue giants rather than blue MS stars. We will return to this issue in §4.1.2.

We over-plot the CMDs with RGB isochrones in Figure 6. The model data plotted here are again from the Padova group (Girardi et al. 2002). In this case, we plot isochrones for models that have the same abundance as in Figure 5 (2% solar), but with the age set to 12.6 Gyr. Hence, these isochrones should show the locations of old stellar populations in the CMDs. We plot both the  $B - V$  and  $V - R$  CMDs in Figure 6, since the latter shows the putative RGB in Leo P with much better definition. We exhibit the model RGBs for the same four distances used in Figure 5: 0.5, 1.0, 1.5, and 2.0 Mpc. The model isochrones with distances between 1.5 and 2.0 Mpc appear to provide the best match for the observations. We discuss our distance determination methods in the following section.

In addition to the photometry of the individual stars, we carried out aperture photometry of the entire galaxy.

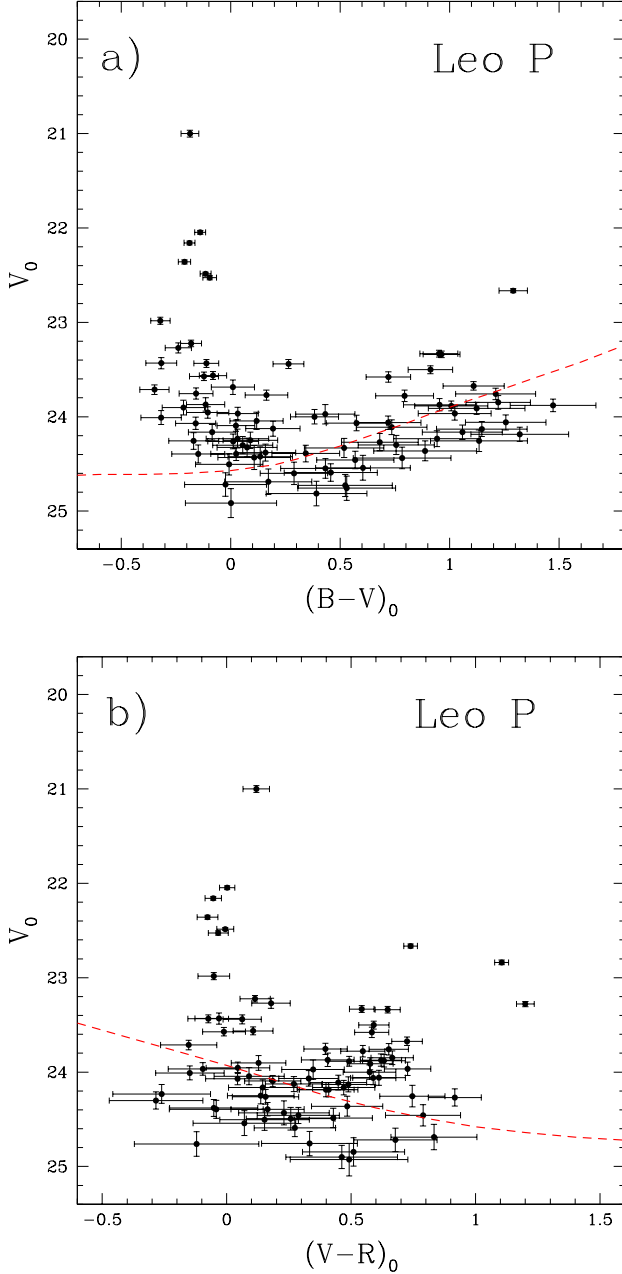


FIG. 3.— Color-magnitude diagrams of the resolved stars in Leo P. The left plot shows  $(B-V)_0$  color, while the right shows  $(V-R)_0$ . Due to the varying depths of the BVR images, the B-V CMD shows better definition of the MS, whereas the V-R plot shows the RGB more clearly. The dashed curves indicate the 50% completeness level for our data.

We first masked bright foreground stars that might contaminate our measurements, then measured the flux in a  $100''$  diameter circular aperture that encompassed the galaxy. The total apparent magnitude of the system is  $V_0 = 16.89 \pm 0.01$  and the broadband colors are  $(B-V)_0 = 0.36 \pm 0.02$  and  $(V-R)_0 = 0.49 \pm 0.01$ . Based on Figure 4, we expect the foreground contamination of our total magnitudes and colors to be quite small. For example, if the light of all the stars present in the comparison fields shown in Figures 4c and 4d was removed from the to-

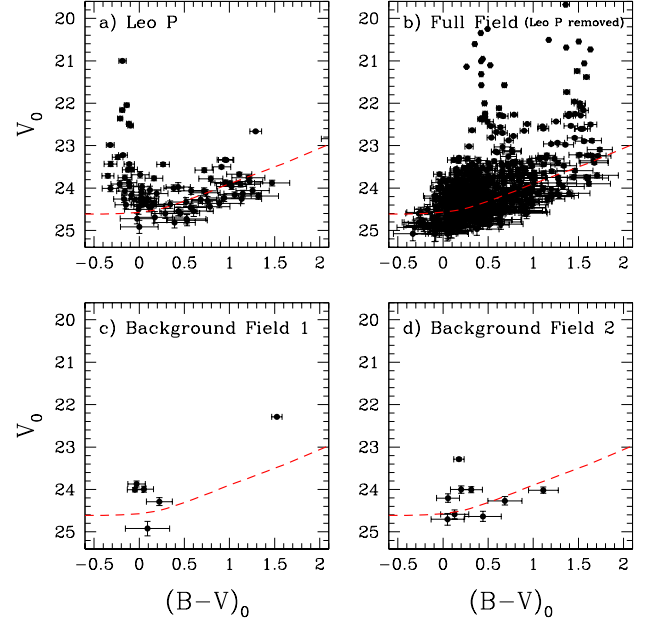


FIG. 4.— CMDs for (a) Leo P, with the same data as shown in Figure 3a; (b) the full CCD image that contains Leo P, but with the stars from the Leo P region excluded; (c) and (d) two background comparison fields with the same area as the Leo P photometry but located far from the galaxy. The strong upper MS identified in Leo P is totally absent from the surrounding field, as indicated by the complete lack of stars with  $(B-V)_0 \leq 0.0$  and brighter than  $V_0 \sim 23.6$  in panel (b). The two lower panels indicate that foreground contamination of the Leo P CMD is likely to be minimal.

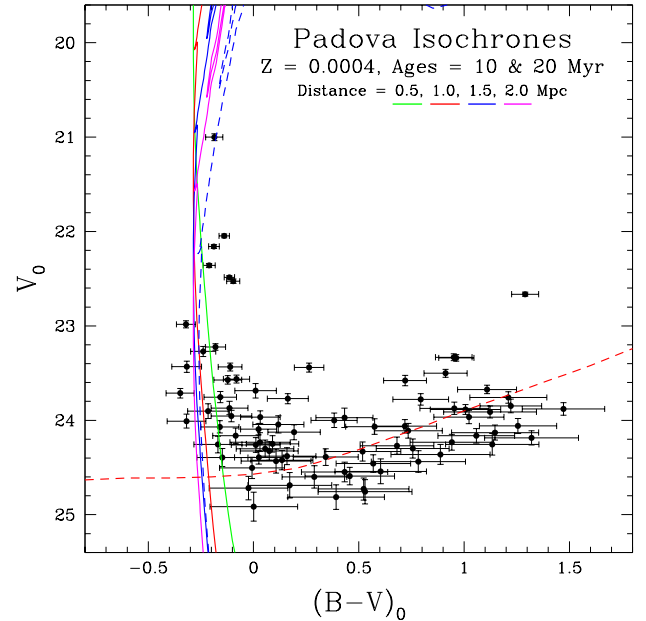


FIG. 5.— CMD constructed from PSF photometry of the stars in Leo P. The data points and 50% completeness line are the same as shown in Figure 3a. Overlaid on the MS stars are isochrones from the Padova group (Girardi et al. 2002) for a 10 Myr old population with  $Z$  of 2% solar and for a range of assumed distances as indicated in the legend (0.5 - 2.0 Mpc). The blue dashed isochrone (for a distance of 1.5 Mpc) shows the effect of increasing the age of the young stellar population to 20 Myr. The blue and magenta isochrones bracket our preferred distance estimate based on the apparent location of the tip of the RGB.



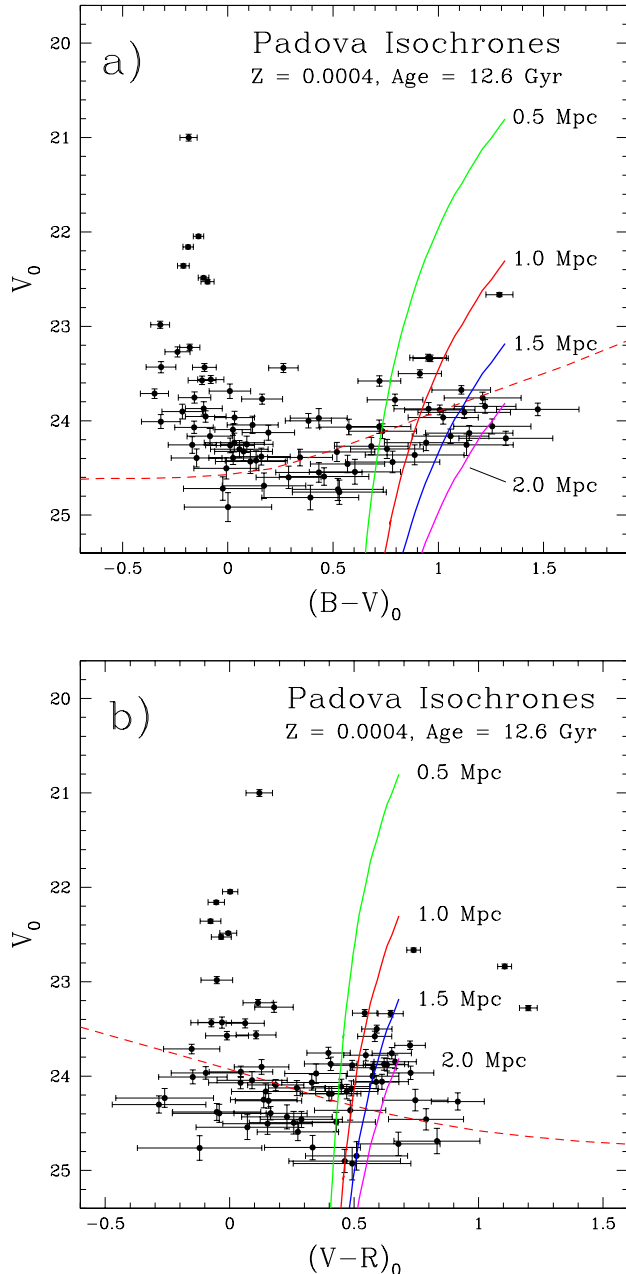


FIG. 6.— Color-magnitude diagrams of the resolved stars in Leo P with red giant branch isochrones superposed. The data are the same as in Figure 3, where the  $V-R$  CMD in panel (b) does a better job of revealing the RGB. The isochrones are from the Padova group (Girardi et al. 2002), and show the locations of the RGB for a 12.6 Gyr old population. We use model isochrones with the same metallicity as those shown in Figure 5 (2% solar). RGBs for four different distances are plotted and labeled, using the same color scheme employed in Figure 5. The isochrones appear to best match the observed RGB in the  $V-R$  CMD for distances between 1.5 and 2.0 Mpc.

tal aperture magnitudes listed above, the corrected  $V_0$  magnitude would change by only 0.014 and 0.013 mag, respectively.

#### 4. DISCUSSION

##### 4.1. Distance Estimate

Distances to most galaxies within  $\sim 10$  Mpc of the Milky Way can be determined with good accuracy using the tip of the red giant branch (TRGB) method (e.g., Lee, Freedman & Madore 1993; Sakai, Madore & Freedman 1996). For galaxies with distances of 1 Mpc or less (i.e., LG members), the TRGB is located at  $V_0 \sim 22.5$  (Salaris & Girardi 2005) or brighter, and accurate distances can be derived using ground-based telescopes. For galaxies at distances of 2 Mpc or greater, the TRGB will be located at  $V_0$  magnitudes fainter than  $\sim 24.0$ , and space-based observations are typically required.

In this section we describe our efforts to use the current observational data to constrain the distance to Leo P. While our data do not allow us to determine a definitive distance, we are able to show that the galaxy is most likely located between 1.5 and 2.0 Mpc from the Milky Way.

##### 4.1.1. TRGB Method

As mentioned in the previous section, the CMD we obtained for Leo P is rather unusual, especially when compared with the CMDs of other nearby dwarf galaxies. In particular, the upper MS is much better defined than the RGB. The latter is the dominant feature in most LG dwarf galaxy CMDs (e.g., Tolstoy et al. 1998; Bellazzini et al. 2004; Irwin et al. 2007; Sand et al. 2009). The TRGB method relies on the detection of a fully populated giant branch to allow for the accurate assessment of the brightness of the RGB tip. Our WIYN observations of Leo P appear to detect the RGB in this system, but the photometric depth is not sufficient to provide a robust measurement of the TRGB. Hence, any TRGB distance we derive can only be taken as approximate.

For metal-poor stellar populations, the TRGB is located at  $(B-V)_0 \sim 1.3$  (Ferraro et al. 1999; Stetson et al. 2005, 2011). The location of the star in Figure 6a with  $V_0 = 22.66$  and  $(B-V)_0 = 1.29$  (Star 7 in Table 1) is consistent with it being at or near the TRGB. Its location in Figure 6b ( $(V-R)_0 = 0.74$ ) further supports this interpretation. If we assume that Star 7 is in fact at the TRGB for Leo P, and using  $M_V(\text{TRGB}) = -2.5$  for the most metal-poor RGB stars (Salaris & Girardi 2005), the inferred distance would be  $D = 1.1$  Mpc. We note, however, that associating the TRGB with this particular star then requires that the RGB in this galaxy is underpopulated in a dramatic way, since the next star along the RGB lies nearly 0.7 mag below the tip. At a distance of 1.1 Mpc, Leo P would have an absolute magnitude of  $-8.3$  and an approximate stellar mass of  $1.5 \times 10^5 M_\odot$ . It would seem highly unlikely that a stellar population with this mass could possess such an underpopulated RGB. No stellar systems with an old population, either globular clusters or dwarf galaxies, are known that are this massive and yet do not have a fully populated RGB (e.g., Okamoto et al. 2012).

A more likely possibility is that Star 7 is a foreground star or a red supergiant rather than a red giant in Leo P. While its location in our CMDs is precisely where one would expect a metal-poor RGB star, it is located very far above the next brightest RGB star (Star 11, with  $V_0 = 23.33$ ). We can test whether Star 7 is likely to be a foreground contaminant by using the data present in Figure 4b. By counting the number of objects that appear in specific magnitude and color ranges of the CMD, then

normalizing that number by the ratio of the area covered by the full comparison field (with Leo P removed) to the area covered by Leo P only, we arrive at an estimate of the number of contaminating objects that might appear in specific magnitude and color regions of the Leo P CMD. Applying this analysis to the area occupied by Star 7 leads to an estimate that one would expect to find a foreground star with a color and brightness comparable to Star 7 in a random field the size of Leo P about 14% of the time. This is large enough that one would not rule out the possibility of Star 7 being a foreground star. Alternatively, and perhaps more likely, Star 7 could be located in Leo P but be an AGB star or possibly a red supergiant star from an intermediate age stellar population.

We note in passing that there are two other very red stars located in the Leo P field with  $(B-V)_o > 2.1$  that we believe are foreground stars. These two stars appear in Figure 6b as having  $(V-R)_o > 1.1$  (they are off the plot to the right in Figure 6a). Given the presence of these two likely foreground objects in the Leo P field, it seems at least conceivable that Star 7 may also fall in this category.

If we assume that Star 7 is not located at the TRGB, we focus next on the group of stars located below  $V_o = 23.3$  and with  $(V-R)_o$  colors between 0.5 and 0.7 in Figure 6b. The brightest of these is Star 11 in Table 1, with  $V_o = 23.33$ ,  $(V-R)_o = 0.54$ , and  $(B-V)_o = 0.95$ . Associating this star with the tip of the RGB leads to an implied distance of 1.5 Mpc. We note that the  $B-V$  colors of Star 11 and the several stars just below it in Figure 6a appear to be too blue for them to be located on the RGB if the distance were closer to 1.5 Mpc. However, in Figure 6b, where the RGB shows better definition due to the smaller photometric errors of the red stars in  $V-R$ , these same stars appear to be consistent with an RGB with a distance anywhere between 1.5 and 2.0 Mpc.

One should ask at this point whether or not the putative upper RGB is heavily contaminated by foreground stars in our data. Following the same analysis method described above, we determined the average surface density of stars located in the color and brightness regime occupied by the top of the RGB in Leo P. For the magnitude range  $V_o = 23.25$  to 24.0 and the  $(B-V)_o$  color range 0.75 to 1.25 (the TRGB portion of the CMD), there are 0.71 stars per Leo P field in our WIYN images. The Leo P CMD has 11 objects in this same region, so the estimated contamination rate for the upper RGB region of the Leo P CMD is approximately 6%. Hence it would appear that one can trust that the current data are not too badly contaminated by foreground objects in the TRGB region of the CMD.

In order to derive a valid TRGB distance, we would require data that are roughly one magnitude deeper than our current photometry. The definition of the RGB present in our current CMD is simply not sufficient to be able to run any sophisticated edge-finding software typically used for ascertaining an accurate TRGB distance. Our estimates above are based on single stars which themselves might be red supergiants or AGB stars. Therefore, it appears that the most robust distance estimate that we can derive for Leo P based on the RGB in our CMDs is 1.5 - 2.0 Mpc. The lower end of this range is established by the location of the brightest star

in Figure 6 that can reasonably be associated with the RGB. The upper end is somewhat softer, but is based on the location of the isochrones in both Figures 6a and 6b in color space. The vast majority of the putative RGB stars in the two CMDs are located blueward of the 2.0 Mpc isochrone. Since the isochrones we are using in these figures are matched to the measured metal abundance of Leo P (Skillman *et al.* 2013), and since differential reddening in the galaxy will only act to push stars to redder colors in the CMDs, we infer that the 2.0 Mpc isochrone indicates a reasonable upper limit for the distance to Leo P.

Recent ground-based imaging observations (K. McQuinn 2013, private communication) have been obtained that reach substantially deeper than our WIYN images. The RGB is definitively detected in these images at the location indicated by our data, and a very preliminary analysis of these new data produce a distance determination that is consistent with our range quoted above. A thorough analysis and presentation of these new data will be forthcoming.

#### 4.1.2. Distance Based on the Bright Blue Stars

Due to the lack of a definitive distance determination from the TRGB method, we explored an alternative approach to estimating the distance. As we show below, it is possible to take advantage of the single H II region present in Leo P to constrain the distance to the galaxy. In the case of this system, nature has provided us with a rather unusual circumstance in which (1) there is one and only one H II region in the galaxy, and (2) the resolved stellar population of luminous blue stars is well delineated by our current observations.

Stars with effective temperatures cooler than  $\sim 20,000$  K, corresponding to a spectral type of B1 or B2, are not capable of producing a significant volume of ionized gas (Osterbrock 1989). The brightest star in Leo P (Star 1) is surrounded by an H II region, while the second brightest (second star in Table 1; hereafter Star 2) is not. Our narrow-band images are sensitive enough to rule out any significant emission around any of the other bright blue stars in Leo P. For example, if Leo P were located at a distance of 1.5 Mpc (e.g., consistent with the TRGB distance found in §4.1.1), we would be able to detect an H II region with an  $H\alpha$  luminosity of only  $1.3 \times 10^{34}$  erg/s, which is 0.1% the  $H\alpha$  luminosity of the Orion Nebula (O'Dell, Hodge & Kennicutt 1999). Hence, we can rule out with a high degree of confidence that there is any significant  $H\alpha$  emission associated with any of the blue stars in Leo P other than Star 1.

We can use the information in the paragraph above to constrain the distance to Leo P. Since it has an H II region around it, Star 1 ( $V_o = 21.00$ ) must have a spectral type of B2 or hotter, while Star 2 ( $V_o = 22.05$ ) must be B3 or cooler. The apparent magnitude difference between these two stars ( $\Delta V_o = 1.05$  mag) further constrains their possible spectral types and luminosities. For example, assuming that Star 2 is a B3V star ( $M_V = -2.00$ ), the observed value of  $\Delta V_o$  would imply that Star 1 is a B0V or O9.5V star ( $M_V = -2.90$  to  $-3.05$ ; all absolute magnitudes for O and B stars are taken from Wegner 2000, using the “smoothed” values). The implied distance to Leo P in this scenario is then  $D = 650$  kpc. The coolest spectral class that Star 1 could have and still



possess an H II region is B2V ( $M_V = -2.30$ ). The observed value of  $\Delta V$  would then lead to Star 2 having an absolute magnitude of  $M_V = -1.25$  and a spectral type of B5V or B6V. In this case the implied distance is  $D = 460$  kpc).

The distances derived above, 460 to 650 kpc, are substantially lower than what we found based on the TRGB method in the previous section. Examination of Figures 6a and 6b appear to rule out distances as small as  $\sim 500$  kpc with high confidence. Why is our distance estimate based on the luminous blue stars so incongruous with the TRGB distance?

Three key assumptions were made in the preceding calculations: (1) the bright blue stars are single stars, (2) they are all on the main sequence, and (3) there is gas in the immediate vicinity of these stars that could be ionized if the surface temperatures of the stars were hot enough. In reality, all three of these assumptions could be incorrect. For example, the stars may not be single stars. It is not uncommon for massive stars to be formed in binary or multiple-star systems (e.g., all four of the Trapezium stars in the Orion Nebula Cluster are multiple-star systems). If we assume that Stars 1 and 2 are both in equal-mass binaries, the inferred distance range would increase to 650 – 910 kpc.

The second assumption – that all the bright blue stars are on the main sequence – might also be erroneous. Recall that while Star 1 is located close to the 10 Myr isochrones in Figure 5, the five blue stars below it (with  $V_o$  between 22.0 and 22.6), including Star 2, are all located to the right of the MS isochrones. These five stars may well be post-MS stars. If this is true, then they may be significantly older than Star 1. Under the assumption that Star 2 is a B3 giant (B3III) rather than a MS star, the inferred distance range for Leo P increases to 590 – 850 kpc if Stars 1 and 2 are both single, and to 830 kpc – 1.20 Mpc if they are equal-mass binaries. Alternatively, if Star 2 were a B3 bright giant (B3II), the corresponding distance range is 780 kpc – 1.15 Mpc for single stars, and 1.10 – 1.62 Mpc for equal-mass binaries. Hence, by simply invoking the assumption that the bright blue stars are evolved stars rather than MS stars, one can derive distances that are consistent with the TRGB distance. Unfortunately, the precise nature of these bright blue stars is unknown, meaning that this method is subject to unreasonably large uncertainties.

Finally, we point out that this distance estimation method relies on the assumption that there is a significant amount of gas in close proximity to the bright blue stars that is capable of being ionized. While this is clearly the case for Star 1, it may not be a valid assumption for the other blue stars, like Star 2. In particular, if the five stars located between  $V_o = 22.0 - 22.6$  with blue colors are all post-MS stars, as suggested in §3 and inferred above, then it would seem likely that they have pushed away the gas associated with their formation episode via stellar winds. It is even possible that they are located in small associations that once included higher-mass stars which ended their lives as supernovae and therefore cleared out the ISM in the immediate vicinity of the groups.

It seems clear that we do not know enough about these individual stars to be able to generate a reliable distance from them using this method. The fact that the lumi-

nosity classes of these stars are unknown, combined with the possibility of binarity or multiplicity, yields distances that range over a factor of nearly four (460 kpc to 1.62 Mpc). It is nevertheless reassuring that the range covered by these possible distances overlaps the distance range inferred from the TRGB method.

#### 4.1.3. Summary of Distance Estimates

We summarize the current status of the distance estimate for Leo P as being uncertain. We adopt a distance of 1.5 to 2.0 Mpc, based on the apparent location of the tip of the RGB in our CMDs. Our attempt to use the bright blue stars that have robust photometry to constrain the distance leads to a distance range that is unacceptably large, although it is consistent with our TRGB estimate under the assumption that at least some of the blue stars present in the galaxy are post-MS objects. We conclude that an unequivocal distance determination is not possible with the current data, and that deeper high-resolution imaging data are required to arrive at a more precise value of the distance. Such data have been obtained recently (K. McQuinn, private communication), and appear to corroborate our distance estimate.

It is appropriate to note that Giovanelli *et al.* (2013) used a completely independent method to estimate the distance to Leo P. Using the baryonic Tully-Fisher relation (e.g., McGaugh 2012) and the observed rotation velocity of the galaxy derived from their HI data, Giovanelli *et al.* derive a distance to Leo P of 1.3 (+0.9, -0.5) Mpc. This value is consistent with our distance estimates derived using the TRGB method.

#### 4.2. Galaxy Properties

Although our distance estimate for Leo P is uncertain, it is nevertheless a useful exercise to derive and consider the physical properties of this newly discovered galaxy. For this exercise we assume the range of distances based on our TRGB estimates: 1.5 - 2.0 Mpc. We present a number of observed and derived quantities in Table 2 computed for three different distances: 1.5, 1.75, and 2.0 Mpc. The observed quantities, obtained from the optical observations presented in the current paper, include the right ascension and declination of the H II region in Leo P, the integrated  $V_o$  magnitude plus  $(B-V)_o$  and  $(V-R)_o$  colors and their errors, and the total  $H\alpha$  flux of the H II region. We use the assumed distances to compute the absolute magnitude, optical diameter, and stellar and H I mass estimates for the galaxy. Stellar masses are derived using the methodology of Bell & de Jong (2001), and the H I mass estimate uses the H I flux from Giovanelli *et al.* (2013). We also derive the  $H\alpha$  luminosity of the single H II region present in Leo P after applying the Schlegel *et al.* (1998) correction for Galactic absorption to our observed  $H\alpha$  flux.

The physical properties of Leo P listed in Table 2 make it clear that this is an interesting system. If we adopt for this discussion a distance of  $1.75 \pm 0.25$  Mpc, then the picture that emerges is one of a very low-luminosity dwarf galaxy ( $M_V = -9.3 \pm 0.3$ ; diameter =  $760 \pm 90$  pc) that is also extremely gas rich. It has an H I mass of  $9.4 \times 10^5 M_\odot$  and an H I-to-stellar mass ratio  $M_{HI}/M_* \sim 2.6$  (the latter number being independent of the distance). It is significantly less luminous than other gas-rich dwarfs like Leo A and Phoenix ( $M_V = -12.1$  and  $-9.9$ , respectively;

TABLE 2  
PROPERTIES OF LEO P

Parameter	Value		
RA – H II region (J2000)	10:21:45.1		
DEC – H II region (J2000)	18:05:17.2		
$V_o$ magnitude	$16.89 \pm 0.01$		
$(B-V)_o$ color	$0.36 \pm 0.02$		
$(V-R)_o$ color	$0.49 \pm 0.01$		
$F_{H\alpha}$ [erg/s/cm <sup>2</sup> ]	$(1.71 \pm 0.03) \times 10^{-14}$		

Distance-Dependent Properties:			
Distance D (assumed) [Mpc]	1.5	1.75	2.0
$M_V$	−9.0	−9.3	−9.6
Diameter [pc]	650	760	870
$L_{H\alpha}$ [erg/s]	$4.8 \times 10^{36}$	$6.6 \times 10^{36}$	$8.6 \times 10^{36}$
$L_V$ [ $L_\odot$ ]	331,000	450,000	588,000
Stellar Mass [ $M_\odot$ ]	269,000	366,000	479,000
H I Mass [ $M_\odot$ ]	689,000	937,000	1,224,000

McConnachie 2012), and hence represents the least luminous/massive system in the local universe known to have current star formation. The star formation rate (SFR) implied by the  $H\alpha$  luminosity is  $\log(\text{SFR}) = -4.27$ , assuming the Kennicutt (1998) conversion factor. This value, while quite low in an absolute sense, places Leo P slightly *above* the observed trend line in the SFR– $L_B$  relation derived from  $H\alpha$  fluxes of galaxies in the Local Volume (e.g., Lee et al. 2009; Karachentsev & Kaisin 2010). By comparison, only one other galaxy with  $M_V$  fainter than approximately  $-10.6$  in the two samples cited above shows evidence for current star formation (as indicated by detected  $H\alpha$  emission).

While the current ground-based photometric data do not allow for a detailed analysis, we can still infer much useful information about the stellar populations present in Leo P. The optical appearance (Figure 1) is dominated by the young, bright blue stars that are clustered in the southern portion of the galaxy. The implied age of Star 1, the central star in the single H II region, is no more than 10–15 Myr assuming that it is a MS star. It seems possible that at least some of the bright blue stars seen in Leo P are older than Star 1 and have evolved off of the MS. These stars could be more than 30 Myr old. This age makes it possible that they were created in an earlier phase of the same event that spawned Star 1, i.e., there may well be linkage between the star-formation events that created all of the luminous blue stars currently seen in Leo P. Whether there is a second intermediate-age population (e.g., with an age of a few-to-several hundred Myr) is unclear from the current data. There was certainly star formation in the distant past in Leo P, since there is clearly a population of red giants present.

One can speculate about what Leo P will look like in the optical in  $\sim 500$  Myr, when all of the bright blue stars will have ended their stellar lives. At that point, and assuming no additional star formation takes place, the southern high-surface-brightness portion of the galaxy will more nearly resemble the current northern low-surface-brightness region. It is not clear whether Leo P would be recognizable (or detectable) as a galaxy

in the optical after 500 Myr, especially if star formation were to cease. Conversely, what did Leo P look like several tens of millions of years in the past? The degree of brightening associated with the recent episode of star formation suggests that there could be other objects similar to Leo P in the local universe lying just below the level of easy detectability at optical wavelengths. Future deep searches of apparently starless H I clouds of the type detected by ALFALFA (Giovanelli et al. 2010, 2013) might well uncover additional examples of low-stellar-mass dwarf galaxies.

The single H II region in Leo P has an  $H\alpha$  luminosity of roughly 50% that of the Orion Nebula (O’Dell, Hodge & Kennicutt 1999) if the 1.75 Mpc distance is assumed. This luminosity is consistent with the ionizing flux being contributed by a single O7 or O8 type star. Our group has obtained spectroscopy of this H II region that reveals a strong emission-line spectrum indicative of a very metal-poor ISM. A full nebular analysis provides an estimate of the oxygen abundance of  $\log(\text{O}/\text{H})+12 \sim 7.1\text{--}7.2$  ( $\sim 2\%$  of the solar value), making Leo P one of the lowest metallicity galaxies known. The details of the spectral analysis of Leo P are presented by Skillman *et al.* (2013).

Despite our incomplete understanding of Leo P, it is still possible to speculate about the evolutionary status of this system. It would appear likely that this galaxy has not passed too close to the Milky Way or Andromeda (yet), since otherwise it is difficult to understand how it could have retained its gas despite its extremely low mass. Whether Leo P has maintained this amount of gas mass since its initial collapse or has accreted most of it more recently is a key question. Its apparent location outside of the LG places it in a relatively benign environment, far beyond the virial radius of either of the giant LG galaxies. Given this location, what process can be invoked to explain its recent episode of star formation? It would appear to be relatively isolated, unless its distance is much lower than we have estimated in the current paper. We note in passing that Leo P is located close on the sky ( $\sim 7^\circ$  away) to Leo I. Furthermore, Leo

I has an observed velocity very similar to Leo P (285 km/s and 264 km/s, respectively). However, Leo I has a secure distance determination of  $\sim 250$  kpc (Bellazzini et al. 2004), which rules out any physical connection between the two. According to McConnachie (2012), Leo I is possibly not gravitationally bound to the Milky Way, but its location and velocity are consistent with it being bound to the LG. Despite its low velocity of  $137 \text{ km s}^{-1}$  in the LG reference frame (Giovanelli et al. 2013), the inferred distance to Leo P makes it unlikely that it is bound to the LG. It would appear that its relative isolation has allowed Leo P to survive and retain its gas since its initial formation. Its relatively pristine nature seems likely to be an outcome of this isolation.

## 5. SUMMARY

We have presented optical observations of the dwarf galaxy Leo P, which was discovered by the ALFALFA H I survey (Giovanelli et al. 2013). Star-forming activity is ongoing in Leo P, as revealed by the detection in our data of a number of luminous blue stars and an H II region apparently ionized by a single star. Those observations and evidence of a RGB constrain the distance to the galaxy to be between 1.5 and 2.0 Mpc. The definition of the upper end of the RGB in our data is poor, making a precise distance determination impossible with the current data set. Additional observations will be required to more accurately characterize Leo P's RGB and to obtain a definitive distance. The limits provided by

our data are sufficient to indicate that Leo P is probably located outside the LG in the Local Volume. Those limits and the measurement of an ultra-low metallicity (Skillman et al. 2013) indicate that Leo P is an extreme object which may well have the lowest mass and luminosity of any star-forming galaxy known. The ALFALFA survey is finding other HI sources that resemble Leo P (Adams et al. 2013), providing an exploratory entry to the regime of the lowest mass, most pristine galaxies.

Support for KLR and MDY was provided by an NSF Faculty Early Career Development (CAREER) award (AST-0847109; PI: Rhode). The ALFALFA team at Cornell is supported by NSF grants AST-0607007 and AST-1107390 to RG and MPH and by grants from the Brinson Foundation. EAKA is supported by an NSF predoctoral fellowship. JMC is supported by NSF grant AST-1211683. We thank the staff of the WIYN Observatory and Kitt Peak National Observatory for their assistance with obtaining the optical data for this study. We acknowledge the insightful comments from an anonymous referee that greatly improved this paper. This research has made use of the NASA/IPAC Extragalactic Database (NED) which is operated by the Jet Propulsion Laboratory, California Institute of Technology, under contract with the National Aeronautics and Space Administration.

## REFERENCES

- Adams, E. A. K., Giovanelli, R., Haynes, M. P. 2013 ApJ, 768, 77  
 Armandroff, T. E., Davies, J. E., & Jacoby, G. H. 1998, AJ, 116, 2287  
 Bell, E. F., & de Jong, R. S. 2001 ApJ, 550, 212  
 Bell, E. F., Slater, C. T., & Martin, N. F. 2011 ApJL, 742 L15  
 Bellazzini, M., Gennari, N., Ferraro, F. R., & Sollima, A. 2004 MNRAS, 354, 708  
 Belokurov, V., Zucker, D. B., Evans, N. W., et al. 2007 ApJ, 654, 897  
 Blitz, L., Spergel, D. N., Teuben, P. J., Hartmann, P. J. & Burton, W. B. 1999 ApJ, 514, 818  
 Braun, R. & Burton, W. B. 1999 A&A 341, 437  
 Canterna, R., & Flower, P. J. 1977 ApJL, 212, L57  
 Ferraro, F. R., Messineo, M., Fusi Pecci, F., et al. 1999 AJ, 118, 1738  
 Giovanelli, R., Haynes, M. P., Kent, B. R., et al. 2005 AJ, 130, 2598  
 Giovanelli, R., Haynes, M. P., Kent, B. R. & Adams, E. A. K. 2010 ApJ, 708, L22  
 Giovanelli, R., Haynes, M. P., Adams, E. A. K., et al. 2013 AJ, submitted  
 Girardi, L., Bertelli, G., Bressan, A., et al. 2002 A&A, 391, 195  
 Haynes, M. P., Giovanelli, R., Martin, A. M., et al. 2011 AJ, 142, 170  
 Irwin, M. J., Belokurov, V., Evans, N. W., et al. 2007 ApJL, 656, L13  
 Karachentsev, I. D., & Kaisin, S. S. 2010 AJ, 140, 1241  
 Karachentsev, I. D., Karachentseva, V. E., Suchkov, A. A., & Grebel, E. K. 2000 A&AS, 145, 415  
 Kennicutt, R. C., Jr. 1998, ARAA, 36, 189  
 Landolt, A. U. 1992 AJ, 104, 340  
 Lee, J. C., Kennicutt, R. C., Jr., Funes, J. G., Sakai, S., & Akiyama, S. 2009 ApJ, 692, 1305  
 Lee, M. G., Freedman, W. L., & Madore, B. F. 1993 ApJ, 417, 553  
 Mateo, M. L. 1998 ARAA, 36, 435  
 Martin, N. F., Ibata, R. A., Irwin, M. J., et al. 2006 MNRAS, 371, 1983  
 McConnachie, A. W. 2012 AJ, 144, 4  
 McGaugh, S. M. 2012 AJ, 143, 40  
 O'Dell, C. R., Hodge, P. W., & Kennicutt, R. C. 1999 PASP, 111, 1382  
 Okamoto, S., Arimoto, N., Yamada, Y., & Onodera, M. 2012 ApJ, 744, 96  
 Oke, J. B., & Gunn, J. E. 1983 ApJ, 266, 713  
 Osterbrock 1989, *Astrophysics of Gaseous Nebulae and Active Galactic Nuclei* (Mill Valley, University Science Books)  
 Sakai, S., Madore, B. F., & Freedman, W. L. 1996 ApJ, 461, 713  
 Salaris, M., & Girardi, L. 2005 MNRAS, 357, 669  
 Sand, D. J., Olszewski, E. W., Willman, B., et al. 2009 ApJ, 704, 898  
 Schlegel, D. J., Finkbeiner, D. P., & Davis, M. 1998 ApJ, 500, 525  
 Skillman, E. D., Salzer, J. J., Berg, D. A., et al. 2013 AJ, in press  
 Stetson, P. B. 1987 PASP, 106, 250  
 Stetson, P. B., Davis, L. E., & Crabtree, D. R. 1990, *CCDs in Astronomy* (ASP Conf. Ser. 8), ed. G. Jacoby (San Francisco, CA: ASP), 289  
 Stetson, P. B., Catelan, M., & Smith, H. A. 2005 PASP, 117, 1325  
 Stetson, P. B., Monelli, M., Fabrizio, M., et al. 2011, *The Messenger*, 144, 32  
 Tolstoy, E., Gallagher, J. S., Cole, A. A., et al. 1998 AJ, 116, 1244  
 Tolstoy, E., Hill, V., & Tosi, M. 2009 ARAA, 47, 371  
 Wegner, W. 2000 MNRAS, 319, 771  
 Whiting, A. B., Hau, G. K. T., Irwin, M., & Verdugo, M. 2007 AJ 133, 715  
 Willman, B., et al. 2005 ApJL, 626, L85  
 Young, L. M., Skillman, E. D., Weisz, D. R., Dolphin, A. E. 2007 ApJ, 659, 331